

Hydrodynamical simulations of coupled and uncoupled quintessence models II: Galaxy clusters

Edoardo Carlesi,¹ ^{*} Alexander Knebe,¹ Geraint F. Lewis,² Gustavo Yepes¹

¹*Departamento de Física Teórica, Universidad Autónoma de Madrid, 28049, Cantoblanco, Madrid, Spain*

²*Sydney Institute for Astronomy, School of Physics, The University of Sydney, NSW 2006, Australia*

Accepted XXXX . Received XXXX; in original form XXXX

ABSTRACT

We study the $z = 0$ properties of clusters (and large groups) of galaxies within the context of interacting and non-interacting quintessence cosmological models, using a series of adiabatic SPH simulations. Initially, we examine the average properties of groups and clusters, quantifying their differences in Λ CDM, uncoupled Dark Energy (uDE) and coupled Dark Energy (cDE) cosmologies. In particular, we focus upon radial profiles of the gas density, temperature and pressure, and we also investigate how the standard hydrodynamic equilibrium hypothesis holds in quintessence cosmologies. While we are able to confirm previous results about the distribution of baryons, we also find that the main discrepancy (with differences up to 20%) can be seen in cluster pressure profiles. We then switch attention to individual structures, mapping each halo in quintessence cosmology to its Λ CDM counterpart. We are able to identify a series of small correlations between the coupling in the dark sector and halo spin, triaxiality and virialization ratio. When looking at spin and virialization of dark matter haloes, we find a weak (5%) but systematic deviation in fifth force scenarios from Λ CDM.

Key words: methods: N -body simulations – galaxies: haloes – cosmology: theory – dark matter

1 INTRODUCTION

Galaxy clusters are the largest bound objects in the Universe, with properties arising from the complex interplay between large scale gravitational dynamics and gas physics. For this reason, they provide a unique laboratory for probing cosmological models on astrophysical scales, and hence to constrain the nature of dark energy (see e.g. Samushia & Ratra 2008; Abdalla et al. 2010; Carlesi et al. 2011; De Boni et al. 2011; Baldi 2012; Allen et al. 2011; Bisnovatyi-Kogan & Chernin 2012). Due to the intrinsic complexity of the processes involved, to gain theoretical insight into the formation and evolution of galaxy clusters, we have to employ computationally expensive hydrodynamical N -body simulations (see Kravtsov & Borgani 2012, for a comprehensive review), and in recent years this approach has been successfully used to describe a large number of observational properties such as X-ray temperatures, gas fractions, Sunyaev-Zel’dovich effect and pressure profiles (Nagai et al. 2007; Croston et al. 2008; Arnaud et al. 2010; Sembolini et al. 2013).

In an initial study Carlesi et al. (2013) (hereafter Paper I) we studied the relation between haloes and their environment, in this work we turn to basic properties of galaxy clusters in the framework of interacting and non-interacting quintessence cosmologies; such cosmologies have been developed to solve the fine-tuning problems

of Λ CDM (see Wetterich 1995; Caldwell et al. 1998; Zlatev et al. 1999; Amendola 2000; Mangano et al. 2003) and their observational properties have been constrained in the background and linear regime (Amendola & Quercellini 2003; Pettorino et al. 2012; Chiba et al. 2013), as well as in the highly non-linear regime by means of N -body simulations (Macciò et al. 2004; Nusser et al. 2005; Baldi & Pettorino 2011; Baldi 2012; Li & Barrow 2011; Baldi & Salucci 2012; Carlesi et al. 2012). In this paper, we will further examine our cosmological simulations, including standard Λ CDM, a free quintessence model with a Ratra-Peebles (Ratra & Peebles 1988) self interaction potential (uDE, uncoupled Dark Energy) and three quintessence models interacting with the dark matter sector (coupled Dark Energy, cDE033, cDE066 and cDE099). The latter set of cDE models all implements a Ratra-Peebles scalar field potential and differ in the value of the coupling parameter β_c only.

Our aim is to establish links between this class of models and a set of observable properties of galaxy clusters, firstly grouping the clusters of galaxies in each simulation into homogeneous samples and link their properties to the cosmological framework. We also focus on individual structures, cross-correlating them across the different simulations and understanding how these dark energy models influence their properties on an object-by-object basis. In practice, this will reveal how structures forming from the same initial conditions, and hence in similar environments, are affected by the global cosmological model.

* E-mail: edoardo.carlesi@uam.es

Table 1. Values of the coupling and potential used for the uDE and cDE models.

Model	V_0	α	β_c
uDE	10^{-7}	0.143	–
cDE033	10^{-7}	0.143	0.033
cDE066	10^{-7}	0.143	0.066
cDE099	10^{-7}	0.143	0.099

The paper is structured as follows: In Section 2 we will briefly introduce the physics of the models as well as their implementation in an N -body code. Section 3 discusses some of the most important features characterizing galaxy clusters in uDE and cDE scenarios, while in Section 4 we cross correlate them. In Section 5 we present a summary of our most important findings and outline the future directions of our work.

2 MODELS AND SIMULATIONS

Here, we briefly review some of the general mathematical features of the models studied and their numerical implementation. We refer the reader to Paper I and references therein for a more detailed discussion.

2.1 Cosmological models

Quintessence is a form of dark energy based on a cosmological scalar field, ϕ , with a Lagrangian that takes the form:

$$L = \int d^4x \sqrt{-g} \left(-\frac{1}{2} \partial_\mu \phi \partial^\mu \phi + V(\phi) + m(\phi) \psi_m \bar{\psi}_m \right) \quad (1)$$

where we allow ϕ to interact with the matter field ψ_m through the dark matter particles' mass term, $m(\phi) \psi_m \bar{\psi}_m$.

The focus of this present study are interacting and non-interacting quintessence models with a so called Ratra-Peebles (see Ratra & Peebles 1988) self interaction potential:

$$V(\phi) = V_0 \left(\frac{\phi}{M_p} \right)^{-\alpha} \quad (2)$$

where M_p is the Planck mass while V_0 and α are two constants whose values can be fixed by fitting the model to observational data (see Wang et al. 2012; Chiba et al. 2013). While in uDE the mass term in Eq. (1) is $m(\phi) = m_0$, with no interaction taking place in the dark sector; in the latter class of models we assume that the masses of dark matter particles evolve according to:

$$m(\phi) = m_0 \exp \left(-\beta_c(\phi) \frac{\phi}{M_p} \right) \quad (3)$$

causing an energy transfer from DM to DE due to the minus sign in front of the coupling. In our simulations we have assumed a constant interaction term $\beta_c(\phi) = \beta_{c0}$.

2.2 N -body settings

Implementing quintessence into a standard N -body solver requires a series of modifications that depend on the nature of the specific model. Under the assumption of a very light scalar field, dark energy clustering can be neglected, so that quintessence only acts at the background level, leading to a different rate of expansion

Table 2. Cosmological parameters at $z = 0$ used in the Λ CDM, uDE, cDE033, cDE066 and cDE099 simulations.

Parameter	Value
h	0.7
n	0.951
Ω_{dm}	0.224
Ω_b	0.046
σ_8	0.8

with respect to the standard Λ CDM case. While accounting for the changes in $H(z)$ is sufficient to properly simulate uDE cosmology, cDE models require a few additional modifications to be introduced, to take into account fifth force effects on the dark matter sector.

We implemented these features into the Tree-PM code GADGET-2 (Springel 2005) following the algorithm of Baldi et al. (2010). To improve computational efficiency, $H(z)$, $m(z)$ and $\phi(z)$ are being read from a series of user provided tables and not calculated "on the fly", generating them using a customized version of the Boltzmann solver, CMBEASY (Doran 2005). Proper initial conditions that take into account modified power spectra and growth factors have been generated suitably modifying the N-GENIC code, for 2×1024^3 gas and dark matter particles in a $250h^{-1}$ Mpc box. Gas physics has been simulated using the publicly available SPH solver of GADGET-2, smoothing over $N_{sph} = 40$ nearest neighbours to obtain the continuous fluid quantities and assuming a standard adiabatic relation $P \propto \rho^\gamma$ with $\gamma = \frac{5}{3}$, thus neglecting radiative effects. All of the non-standard implementations have been carefully tested, to ensure that the new numerical techniques do not introduce systematic errors.

2.3 Halo catalogues

Bound structures in our simulations have been identified using AHF¹ (Gill et al. 2004; Knollmann & Knebe 2009), which has been modified to take into account the influence of the different cosmologies. We use the equation

$$M_\Delta = \Delta \times \rho_c(z) \times \frac{4\pi}{3} R_\Delta^3. \quad (4)$$

to define M_Δ as the total mass enclosed within a radius containing an average overdensity of Δ times the critical density of the universe (which needs to be properly taken into account in each different cosmological model).

From the sample of haloes identified this way we restricted our analysis to the virialized structures satisfying

$$\frac{2K}{|U|} - 1 < 0.5 \quad (5)$$

where K is the kinetic and U the potential energy (Prada et al. 2012). We therefore ensure that unrelaxed structures (probably undergoing major mergers) do not bias our analysis. Even though this can be used in combination with other criteria (Macciò et al. 2007; Prada et al. 2012), we checked that their implementation would not affect our sample and thus adopted exclusively this one. We also mention here that we do not expect the above condition to introduce any systematic bias into our object samples drawn from the

¹ <http://www.popia.ft.uam.es/AHF>

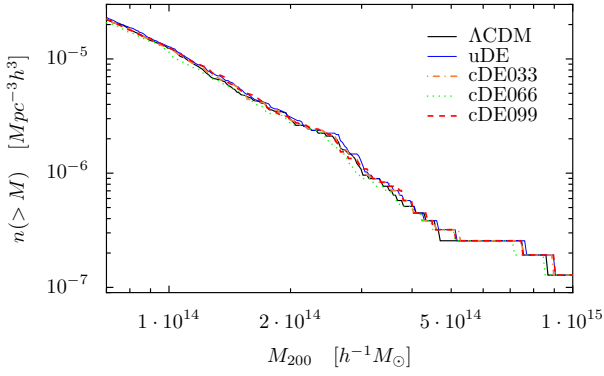


Figure 1. Cluster mass function for Λ CDM, uDE, cDE033, cDE066 and cDE099. Although the statistics in this mass regime is small, abundances are very similar for all the models.

Table 3. Number of (relaxed) galaxy clusters and large groups at $z = 0$ for different mass thresholds, found in the Λ CDM, uDE, cDE033, cDE066 and cDE099 simulations.

Model	$N(> 7 \times 10^{13} h^{-1} M_{\odot})$	$N(> 10^{14} h^{-1} M_{\odot})$
Λ CDM	338	190
uDE	350	198
cDE033	334	193
cDE066	321	178
cDE099	340	193

cDE simulations: even though – as we will be discussed in Section 4.1 – additional couplings in the dark sector introduce a shift into the standard virial relation, this effect is of the order $\approx 5\%$ and thus negligible with respect to the size of the deviations removed using Eq. (5).

3 GENERAL PROPERTIES OF GALAXY CLUSTERS

We first study properties of structures with mass $M > 7 \times 10^{13} h^{-1} M_{\odot}$, which in our simulations are composed of more than 10^5 dark matter and gas particles. This sample includes both clusters and large groups, and we will either use the whole set or a smaller subset of it depending on the kind of properties to be analyzed. In fact, due to the sharp decline of the upper end of the cumulative halo mass function (shown in Fig. 1), a 30% reduction in the mass threshold leads to a twofold increase in the cumulative number of objects, which can be useful for statistical purposes. Complementary to the cumulative mass function (Fig. 1) we also list the total number of clusters and large groups in each cosmology in Table 3. It is evident that different models deliver very similar results (as discussed in Paper I), although we probably need a larger computational volume for a proper quantification of the magnitude of this effect, minimizing the impact of cosmic variance.

3.1 $T_X - M$ relation

Cluster X-ray temperatures are an extremely important observational proxy for halo mass (Ettori et al. 2004; Muanwong et al.

2006; Nagai et al. 2007) to which they are related via a scaling relation of the form

$$M(T_X) = M_0 \left(\frac{T_X}{3 \text{keV}} \right)^{\alpha} \quad (6)$$

where theoretical models (Kaiser 1986; Navarro et al. 1995) predict $\alpha \approx \frac{3}{2}$. We can estimate X-ray temperatures for our simulated objects using three different definitions of T , namely, the mass-weighted temperature T_{mw} , the emission-weighted temperature T_{ew} and the spectroscopic-like temperature (Mazzotta et al. 2004) T_{sl} which reads:

$$T_{mw} = \frac{\sum_i m_i T_i}{\sum_i m_i} \quad (7)$$

$$T_{ew} = \frac{\sum_i m_i \rho_i T_i \Lambda(T_i)}{\sum_i m_i \rho_i \Lambda(T_i)} \quad (8)$$

$$T_{sl} = \frac{\sum_i m_i \rho_i T_i^{1/4}}{\sum_i m_i \rho_i T_i^{-3/4}} \quad (9)$$

where T_i , ρ_i and m_i are the i^{th} gas particle temperature, mass and density, while $\Lambda(T_i)$ is the cooling function, which we assumed to be $\propto T^{1/2}$ (thermal Bremsstrahlung). Only particles of $T > 0.5 \text{keV}$ are included in the computation of the cluster temperatures, to remove the effect of cold flows. In Fig. 2 we show the temperature mass relations for objects larger than $7 \times 10^{13} h^{-1} M_{\odot}$, from which we can see that all the models, regardless of the temperature definition, closely follow the same $M - T$ relation of Eq. (6). This equation has been fitted using M_{500} (which is closely related to the observations Sembolini et al. (2013)) and the three different definitions of T introduced before. In the case of Λ CDM these values are compatible with the findings of Allen et al. (2001); Ettori et al. (2002); Nagai et al. (2007) and Ventimiglia et al. (2008). It is quite clear that the impact of quintessence on this relation is completely negligible. Although, as we will discuss later, cDE models have different effects on the properties and distribution of baryons inside galaxy clusters, it is evident that the scaling of the X-ray temperature with the mass is not affected in the class of quintessence theories under investigation here. This might be due to the integrated nature of the relation, which conceals the details of the underlying matter distribution of each object.

3.2 Radial dark matter profiles

As reported by Baldi et al. (2010); Li & Barrow (2011), the Navarro Frenk White (NFW) profile (Navarro et al. 1996);

$$\rho(r) = \frac{\rho_0}{\frac{r}{r_s} \left(1 + \frac{r}{r_s} \right)^2} \quad (10)$$

provides a good description of the distribution of dark matter inside virialized haloes also in the framework of cDE cosmologies. While in Paper I we already presented an analysis of density profiles for a large number of low mass haloes, our focus here lies with the internal structure of a few, well resolved objects. We fit each (relaxed) halo using the radial density profiles computed by AHE, which provides dark matter density for logarithmically spaced bins assuming a spherically symmetrical distribution. We then compute for each

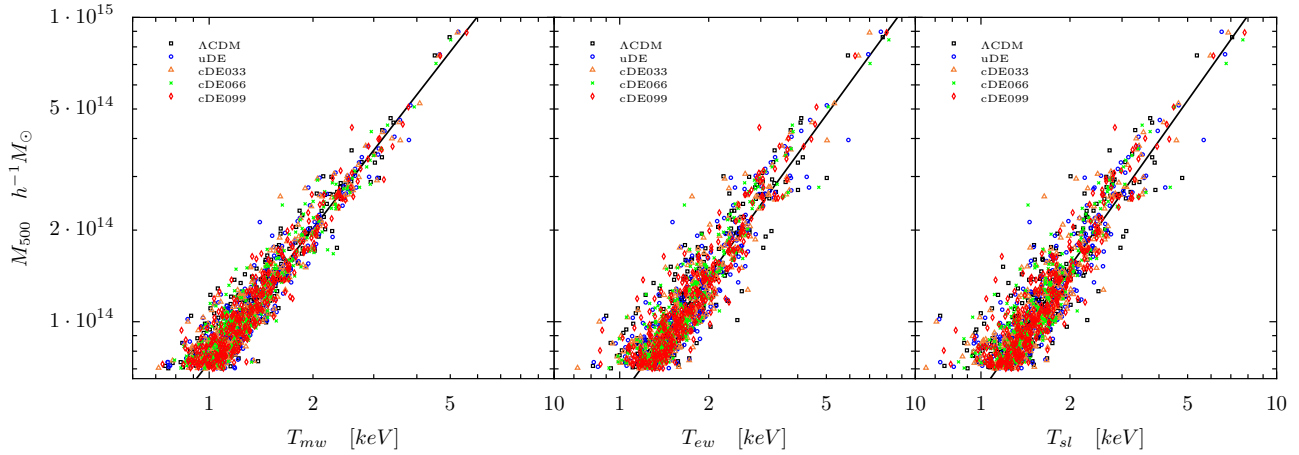


Figure 2. Mass weighted, emission weighted and spectroscopic like temperatures versus M_{500} for objects above $7 \times 10^{13} h^{-1} M_{\odot}$ in all simulations. The solid black lines represents the best fit $M - T$ power law relation for Λ CDM, which closely followed by all cosmological models.

Table 4. Best-fit values to the $M - T_X$, obtained fitting Eq. (6) using M_{500} versus the three temperature definitions T_{mw} , T_{ew} and T_{sl} definitions. The M_{0s} are given in units of $10^{13} h^{-1} M_{\odot}$. All the models follow closely Λ CDM, making this kind of relation a poor proxy for quintessence detection.

Model	M_0^{mw}	α^{mw}	M_0^{ew}	α^{ew}	M_0^{sl}	α^{sl}
Λ CDM	6.31 ± 0.08	1.46 ± 0.03	4.89 ± 0.09	1.33 ± 0.03	5.09 ± 0.09	1.37 ± 0.04
uDE	6.21 ± 0.09	1.47 ± 0.03	4.85 ± 0.07	1.33 ± 0.03	5.05 ± 0.07	1.38 ± 0.03
cDE033	6.29 ± 0.09	1.46 ± 0.03	4.81 ± 0.07	1.36 ± 0.03	4.95 ± 0.08	1.37 ± 0.04
cDE066	6.31 ± 0.08	1.46 ± 0.03	4.96 ± 0.09	1.34 ± 0.03	5.19 ± 0.09	1.38 ± 0.04
cDE099	6.27 ± 0.07	1.45 ± 0.03	4.80 ± 0.09	1.37 ± 0.03	5.03 ± 0.07	1.41 ± 0.03

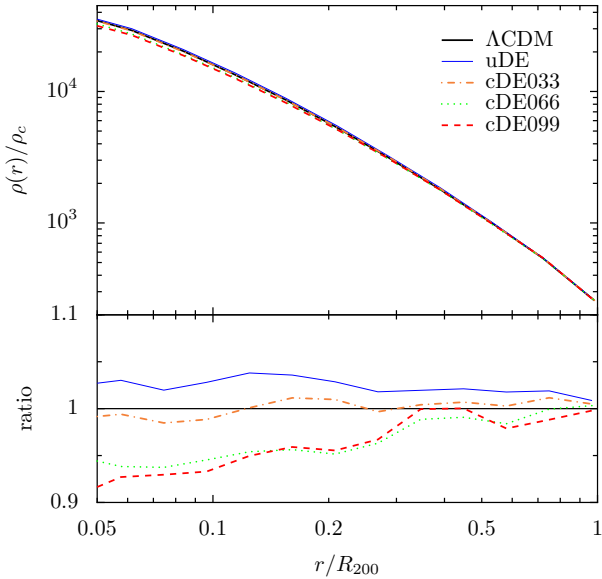


Figure 3. Average dark matter density profile for virialized clusters above $10^{14} h^{-1} M_{\odot}$ as a function of radius. The additional interaction tends to reduce densities towards the halo center, as we can clearly see in cDE099 and cDE066.

halo the corresponding goodness-of-fit Δ^2 (Springel et al. 2008), defined as

$$\Delta^2 = \frac{1}{N_{bins}} \sum_{i=1}^{N_{bins}} (\log_{10}(\rho_i^{(th)}) - \log_{10}(\rho_i^{(num)}))^2 \quad (11)$$

where the ρ_i 's are the numerical and theoretical densities in units of the critical density ρ_c at the i^{th} radial bin.

From the distribution of Δ^2 (not shown here) we can deduce that no substantial difference can be seen in the different cosmologies, that is, the NFW formula of Eq. (10) describes (on average) equally well dark matter halo profiles in Λ CDM as in the other (coupled) dark energy models – something already presented in Paper I, but now extended to larger masses.

We complement this finding with Fig. 3 where we show $\rho(r)/\rho_c$ averaged over all our objects with $M > 10^{14} h^{-1} M_{\odot}$ as a function of distance to the halo centre in units of R_{200} : there, however, it is evident that the innermost regions of the largest cDE clusters are associated with densities $\approx 10\%$ lower than the Λ CDM value. This phenomenon has also been observed and explained – in a different mass range – by Baldi et al. (2010), who attributed it to the extra friction caused by the interaction of dark energy and dark matter, which adds up to the particles' velocities causing a small relative expansion of the halo.

3.3 Radial gas profiles

Due to their large size, galaxy clusters are considered to be a "fair sample" of the Universe, and thus should contain a fraction of baryons close to the cosmic baryon fraction given by Ω_b/Ω_m , where Ω_b measures the total baryonic and Ω_m the total non-relativistic matter content. Acting on the cosmic expansion and thus indirectly on the collapse and formation of large structures, we can expect quintessence to leave an imprint in the gas distribution within them. The relation between dynamical dark energy and the

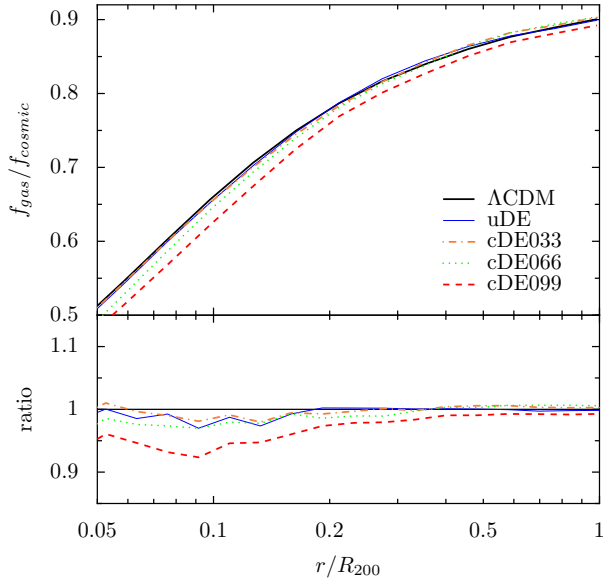


Figure 4. Gas fraction in units of the cosmic baryon fraction as a function of radius averaged for clusters above $10^{14} h^{-1} M_{\odot}$. We observe that the suppression in the value of the gas fraction is stronger towards the central regions and increases with β_c . However, weakly interacting cDE033 and uncoupled uDE are substantially indistinguishable from the standard cosmological model.

baryon content of clusters has been studied by Samushia & Ratra (2008) where they obtained constraints on the slope of the Ratra-Peebles potential (cf. Eq. (2)). Gas dynamics and abundance in coupled dark energy cosmologies have also been studied on slightly different cosmological scales by Baldi et al. (2010); Baldi & Viel (2010); Baldi (2011), finding a correlation between baryon fractions and scalar field coupling to DM.

Here we add to these studies by analyzing the radial distribution of gas and its properties like density, temperature and pressure, focusing on structures with $M_{200} > 10^{14} h^{-1} M_{\odot}$ again, which are composed of more than 3×10^5 gas and DM particles and hence allow us to adequately resolve their internal structure.

Gas fractions In Fig. 4 we show

$$f_{gas} = \frac{M_{gas}(< r)}{M_{tot}(< r)} \quad (12)$$

in units of the cosmic baryonic fraction and averaged over the ≈ 180 most massive galaxy cluster in each simulation. Our Λ CDM results are in agreement with e.g. Sembolini et al. (2013), who found identical results for the shape of $f_{gas}(r)$ in a set of adiabatic Λ CDM clusters. However we clearly observe that the net effect of the coupling is to reduce the baryon content of the cluster in proportion to the value of β_c . The suppression is stronger towards the central regions of the cluster, where the average suppression is $\approx 7\%$ for cDE099 and $\approx 5\%$ in cDE066, while cDE033 and uDE follow closely the values of Λ CDM. At larger radii all results tend to converge to the Λ CDM value of f_{gas} , which is slightly below the value of the cosmic baryon fraction $\Omega_b/\Omega_m = 0.17$. However, we must stress again that due to the absence of radiative cooling these profiles are useful only as far as they allow us to provide a first estimate of the impact of coupling in the dark sector on the (radial distribution of the) gas content of galaxy clusters. And in that regards, our results are in qualitative agreement with the find-

Table 5. Best-fit values to Eq. (14) for the gas density profile averaged over galaxy clusters of $M_{200} > 10^{14} h^{-1} M_{\odot}$. The core radii r_c and r_s are given in units of R_{200} .

Model	β	r_c	r_s	ϵ
Λ CDM	0.43 ± 0.01	0.058 ± 0.002	0.40 ± 0.05	0.41 ± 0.05
uDE	0.41 ± 0.01	0.056 ± 0.002	0.34 ± 0.07	0.38 ± 0.05
cDE033	0.41 ± 0.02	0.053 ± 0.002	0.33 ± 0.07	0.36 ± 0.08
cDE066	0.39 ± 0.01	0.053 ± 0.003	0.33 ± 0.05	0.36 ± 0.05
cDE099	0.42 ± 0.02	0.064 ± 0.004	0.36 ± 0.05	0.35 ± 0.04

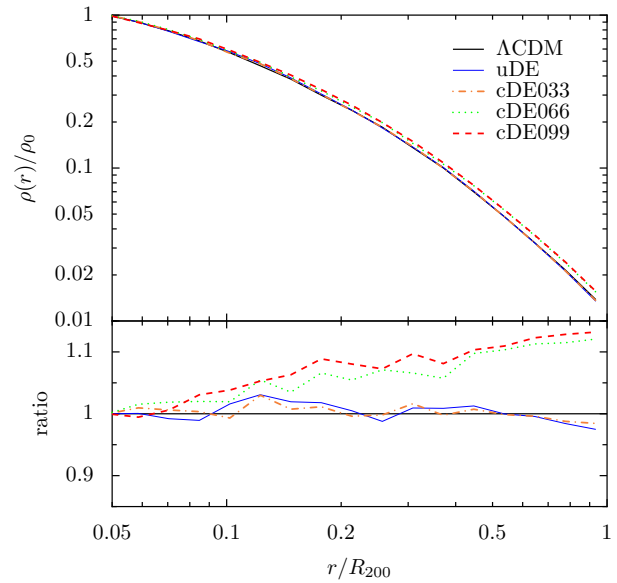


Figure 5. Radial distribution of gas density averaged for clusters above $10^{14} h^{-1} M_{\odot}$, normalized to the central density ρ_0 .

ings of Baldi et al. (2010); Baldi (2011), who also established a link between fifth force and lower baryon fractions for various classes of interacting models, including non-constant coupling models and with different types of self-interaction potentials.

This effect, called baryon segregation, was first analyzed and described in detail in the works of Mainini (2005) and Mainini & Bonometto (2006), where it was explained in terms of the different species' infall velocity towards the centre of the potential well in a spherical top-hat fluctuation. In fact, this happens to be faster for DM than for baryons, since the coupling adds to the gravitational pull in that drives the collapse of the dark matter overdensity. Therefore, gas particles will be relatively less abundant around the central parts of the halo, where they are to be accreted at a slower pace, while their presence in the outer layers is only negligibly affected by this phenomenon.

Density profile After studying how the baryon fraction (which is a combination of gas and dark matter properties) is affected we consider whether the coupling also induces sizeable effects in the gas density profile alone. Under the assumption of hydrostatic equilibrium (which holds to the same degree in both quintessence models and Λ CDM – as we will see in Section 3.5 below) we can derive a simple functional form for the gas density profile

(Cavaliere & Fusco-Femiano 1976), the so called β^2 model:

$$\rho(r) = \rho_0 \left(1 + \left(\frac{r}{r_c} \right)^2 \right)^{-\frac{3}{2}\beta} \quad (13)$$

where r_c is the core radius and ρ_0 is the inner cluster density, which is defined as $\rho(r = 0.05 \times R_{200})$. Observations (Vikhlinin et al. 1999) and simulations (Rasia et al. 2004) have shown that Eq. (13) does not simultaneously reproduce both the inner and outer parts of density distribution of galaxy clusters, even though this model can still be used as a valuable theoretical tool that captures the main characteristics of the intra-cluster medium (ICM) (Arnaud 2009). Hence, for a quantitative comparison of the results for radial distribution of gas densities in the different cosmologies we refer here to a model proposed by Mroczkowski et al. (2009). This was developed for the observational description of X-ray cluster profiles, and is based on the formula proposed in (Vikhlinin et al. 2006), which in turn is an extension of the simple β model. Here we re-write Eq. (13) as:

$$\frac{\rho(r)}{\rho_0} = \frac{1}{\left(1 + \frac{r^2}{r_c^2} \right)^{\frac{3}{2}\beta}} \times \frac{1}{\left(1 + \frac{r^3}{r_s^3} \right)^\epsilon} \quad (14)$$

where the additional multiplicative term on the right contains a new scale radius r_s and power law ϵ , which capture the departure from the standard β model at larger radii. We then compute the average $\rho(r)/\rho_0$ per radial bin (in units of R_{200}), again using all clusters of $M_{200} > 10^{14} h^{-1} M_\odot$. We check that Eq. (14) holds for all the models verifying that the corresponding goodness of fits take comparable values (analogously defined to Eq. (11)); and in Table 5 we show the best-fit parameters; note that we defer from showing the best-fit curves in Fig. 5 again to not overload the plot. The parameters do not seem to show any trend for cDE and uDE models, except for a slightly shallower outer slope ϵ in coupled cosmologies which can be also seen in Fig. 5 where we present the averaged radial gas distribution. We also notice that for our objects β is substantially lower than usually assumed (≈ 0.66), however, this can be easily explained by the fact that our model has two different slopes to account for the two different regimes: this means that, being biased by the core regions of the cluster, where the decrease in density is shallower, β will consequently be smaller.

Fig. 5 further shows clearly that – away from the center of the clusters – the cDE066 and cDE099 gas densities increasingly diverge from the other models, up to more than 10% at the outer edge. As discussed earlier, using the theoretical framework of Mainini (2005); Mainini & Bonometto (2006), these models are characterized by lower baryon fractions in the central regions of the clusters (i.e. a smaller ρ_0 , according to our definition) which on the other hand converge to Λ CDM, cDE033 and uDE in the outer regions. Hence, divergences in $\rho(r)$ for $r \rightarrow R_{200}$ are explained by the small denominator ρ_0 , enhancing even more the gap between the predictions of coupled quintessence cosmologies and the standard model.

Pressure profiles Having analyzed the properties of baryon density distributions, we now consider the pressure profiles, which can be modeled assuming a simple adiabatic relation of the type

$$P(r) = P_0 \rho_{gas}^\gamma(r) \quad (15)$$

² This β must not be confused with β_c , the coupling parameter

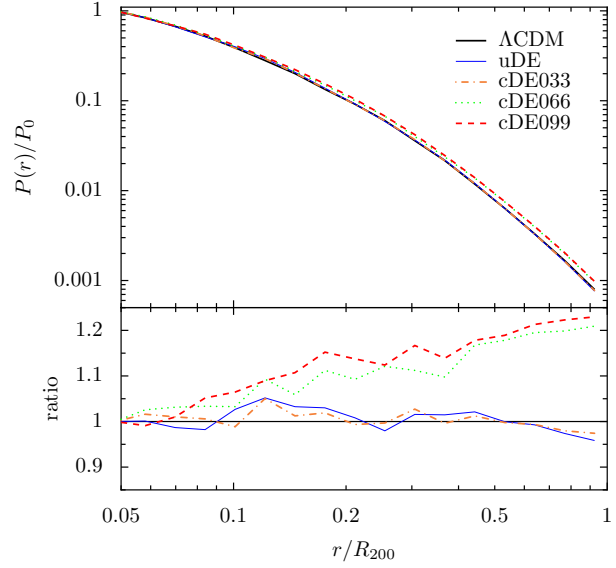


Figure 6. Pressure profiles averaged over clusters above $10^{14} h^{-1} M_\odot$.

where P_0 is an arbitrary normalization constant (which we take to be equal to $P(0.05 \times R_{200})$), and $\gamma = 5/3$ for the case of an adiabatic gas – as assumed in our simulations. Using the densities computed in the previous sub-section, it is straight-forward to obtain the pressure profiles by using Eq. (15); the results are plotted in Fig. 6. It is remarkable that the differences among the models are now much larger (note the enlarged range in the ratio plot), since the discrepancies observed previously are now basically amplified by the adiabatic index γ . Again, this effect increases towards the outer halo edge, where the ratio of $\rho_{gas}(r)$ to the inner density ρ_0 is larger in cDE models due to the under-abundance of gas in the central regions.

Qualitatively, the shapes in Fig. 6 reproduce well the so-called universal pressure profile of galaxy clusters, which can be reconstructed using Sunayev-Zel’dovich effect and X-ray data (Arnaud et al. 2010; Bonamente et al. 2012; Planck Collaboration et al. 2013). However, the errors on the observational results are still larger than the spread among the different models considered here so that for the moment it is not possible to use these dataset to directly constrain quintessence. Moreover, a direct comparison to the data would probably require to relax the unrealistic assumption of completely adiabatic gas and introduce additional effects (such as radiative cooling, star formation, and AGN feedback) to properly simulate the gas physics. In any case, it is clear that gas pressure in cluster does represent an important probe for cDE cosmologies, as the non-linear relation between gas and pressure significantly magnifies the prediction of scarcer gas in the core regions characteristic of these cosmological models.

Temperature profiles Observations have shown (Markevitch et al. 1998; Vikhlinin et al. 2005, e.g.) that galaxy clusters have a declining temperature towards larger radii, in contrast with the simplest isothermal models. The same pattern is seen in our simulations, as the curves in Fig. 7 show, and is in qualitative agreement with the findings of Vikhlinin et al. (2006); Arnaud et al. (2010); Baldi et al. (2012). However, it is known that adiabatic SPH simulations fail to reproduce the inner cool core of galaxy clusters (Kravtsov & Borgani 2012) up to a value

Table 6. Best fit values to a linear relation for the outermost values of the temperature profile. The vertical dashed line denotes the innermost excluded region, where the linear relation does not hold.

Model	A	B
Λ CDM	1.05 ± 0.01	0.61 ± 0.02
uDE	1.10 ± 0.01	0.61 ± 0.02
cDE033	1.10 ± 0.01	0.61 ± 0.02
cDE066	1.11 ± 0.02	0.59 ± 0.01
cDE099	1.11 ± 0.02	0.59 ± 0.01

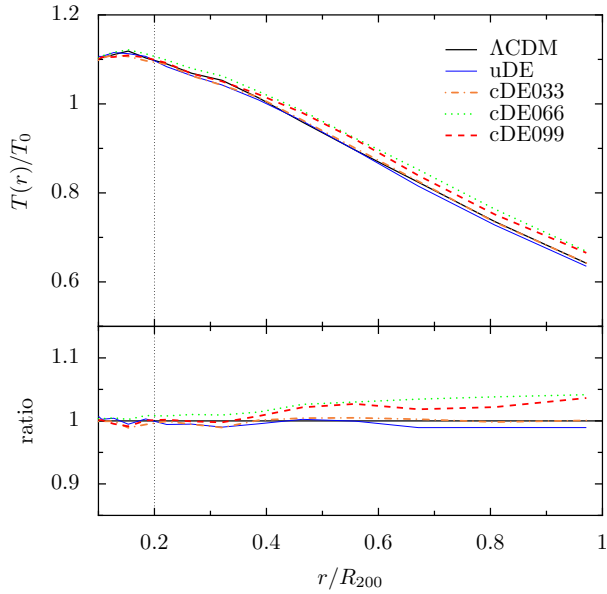


Figure 7. Temperature profiles averaged over clusters above $10^{14}h^{-1}M_{\odot}$.

of $\approx 0.2 \times R_{200}$; this point is marked by a vertical dotted line in Fig. 7.

Following De Grandi & Molendi (2002) and Leccardi & Molendi (2008) we model the outer parts of galaxy clusters using a linear function

$$\frac{T(r)}{T_0} = A - B \left(\frac{r}{R_{200}} - 0.2 \right) \quad (16)$$

where A and B are two free parameters and T_0 is the average temperature for each cluster. We proceed identifying all structures above $10^{14}h^{-1}M_{\odot}$ and fitting Eq. (16) using the gas densities and temperatures for regions of $r > 0.2 \times R_{200}$. The best-fit values are presented in Table 6 while only the numerical results are plotted in Fig. 7. The five profiles are very similar and the largest differences can be seen in the strongest coupled cases of cDE066 and cDE099, where the scaled temperature at the halo edge is $\approx 5\%$ larger than in the other models. However, all the points as well as the best-fit values are still consistent within the error so that this small difference is considered to be not significant. The effect of the coupling is thus marginal in this case, and it seems unlikely that radial temperature measurements alone can provide a mean to distinguish amongst at least the models considered here.

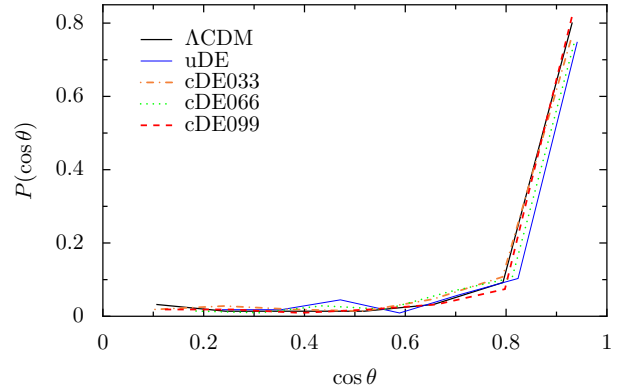


Figure 8. Average cosine of the alignment angle between the gas and dark matter major axes, averaged for objects with $M_{200} > 10^{14}h^{-1}M_{\odot}$.

3.4 Gas alignment to the dark matter halo

We now extend our study to the full 3D distribution of the gas inside the halo, i.e. we are considering the shape of the gas particles spatial distribution. To this extent, we utilize the inertia tensor

$$I_{ij}^{\text{gas}} = \sum_{n_{\text{gas}}} x_{(n),i}^{\text{gas}} x_{(n),j}^{\text{gas}} \quad (17)$$

where $x_{(n),i}^{\text{gas}}$ is the position vector relative to the center of the baryon mass distribution of the n^{th} particle. In the same way we write the halo's inertia tensor

$$I_{ij}^{\text{dm}} = \sum_{n_{\text{dm}}} x_{(n),i}^{\text{dm}} x_{(n),j}^{\text{dm}} \quad (18)$$

which is now given by summing over dark matter particles only. We then diagonalize the two tensors using the two largest eigenvectors \mathbf{e}_1^h and \mathbf{e}_1^b – which are the major axes of the dark matter and baryon distribution, respectively – in what follows. To check whether quintessence has an influence on the relative spatial distribution of gas and dark matter particles we compute

$$\cos\theta = \frac{\mathbf{e}_1^h \cdot \mathbf{e}_1^b}{|\mathbf{e}_1^h \mathbf{e}_1^b|} \quad (19)$$

for all clusters above $10^{14}h^{-1}M_{\odot}$ again. The probability distribution of $\cos\theta$ is shown in Fig. 8, where we can see that all cosmological models follow the same pattern of close alignment between gas and dark matter distributions, although with some scatter among the models at small angles, where $\cos\theta \rightarrow 1$. We note here that our results refer to the gas properties only, and cannot be directly compared to Lee (2010) and Baldi et al. (2011), who looked at galaxy alignment.

3.5 Hydrostatic equilibrium

Observations of galaxy clusters usually assume hydrostatic equilibrium (HSE) to derive their masses. Under this hypothesis, gas and galaxies are both in equilibrium with the binding cluster gravitational potential (Sarazin 1986; Evvard 1990; Bahcall & Lubin 1994). However, this assumption is not always valid and is a major source of uncertainty when deriving observational scaling relations. Many authors (e.g. Ameglio et al. 2009; Lau et al. 2009; Sembolini et al. 2013) found a systematic underestimation of cluster masses within the range 10 – 25% for Λ CDM. This was explained by Lau et al. (2009) and identified as an effect driven by

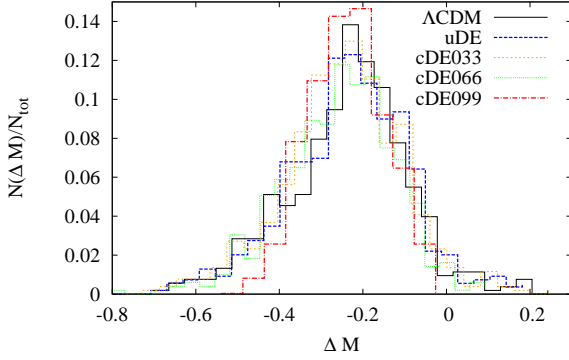


Figure 9. Distribution of $\Delta M = (M_{HSE,200} - M_{200})/M_{200}$, the difference between the cluster mass estimated using the hydrostatic equilibrium assumption and the true mass obtained in the simulations. We computed M_{HSE} for relaxed haloes of $M > 9 \times 10^{13} h^{-1} M_{\odot}$. The distribution of ΔM is peaked around -0.12 for all models, showing no large deviation from the Λ CDM pattern neither in uDE nor in cDE cosmologies.

Table 7. Best fit values to a Gaussian distribution for the ΔM computed under the hypothesis of HSE. While all the models tend to produce similar results, we see that cDE099 has a narrower dispersion around the peak; yet the absence of a comparable effect in the other cDE models indicates that the correlation to the coupling is at best very weak.

Model	ΔM_0	σ
Λ CDM	0.23 ± 0.02	0.35 ± 0.03
uDE	0.24 ± 0.02	0.37 ± 0.04
cDE033	0.22 ± 0.02	0.36 ± 0.04
cDE066	0.23 ± 0.02	0.35 ± 0.03
cDE099	0.23 ± 0.02	0.28 ± 0.03

random gas motion that contribute to the pressure support, which in HSE is used to estimate the mass using the relation

$$M_{HSE}(< r) = -\frac{kT_{mw}r}{Gm_H\mu} \left(\frac{d \ln \rho}{d \ln r} + \frac{d \ln T}{d \ln r} \right). \quad (20)$$

where k is the Boltzmann constant, T_{mw} is the mass weighted temperature, m_H is the hydrogen mass, μ is the hydrogen mass fraction and ρ is the gas density.

We are interested in examining the impact of alternative cosmological scenarios on the above estimation as the effective dark matter gravitational potential is affected by the presence of an additional interaction mediated by the dark energy. To accomplish this we identify relaxed clusters (as defined by Eq. (5)) of $M_{200} > \times 10^{14} h^{-1} M_{\odot}$, and compute for each one of them the function $M_{HSE}(< r)$ using the temperature and pressure profiles. We can then straight-forwardly obtain an estimated total mass $M_{HSE,200}$ simply by using its value at the halo edge R_{200} , defined by Eq. (4).

The distribution of the fractional difference

$$\Delta M = \frac{M_{HSE,200} - M_{200}}{M_{200}} \quad (21)$$

with respects to the true mass as returned by the halo finder is shown in Fig. 9, where we clearly see that this mass estimator has an average negative bias peaked around $\Delta M_0 = -0.22$ and a dispersion $\sigma = 0.34$ for all models (as shown in Table 7), except for cDE099 which shows a slightly more pronounced peak and a

narrower dispersion around it. However, because of the absence of such a trend in the other cDE models and the non-negligible error bars, it appears more likely that this effect is due to a statistical fluctuation.

It is thus safe to state that uDE and cDE cosmologies are not responsible for any additional bias, even though the use of a larger halo sample containing more clusters with $M_{200} > 10^{15} h^{-1} M_{\odot}$ might be needed to test whether this statement really holds at even higher mass scales.

4 CROSS-CORRELATED PROPERTIES OF GALAXY CLUSTERS

Due to our approach of using the same random phases for all models when generating the initial conditions for the simulations we are in the situation of cross-identifying the same objects in all the models. Therefore, focusing on structures forming in the same environments whose evolution is driven by different laws, we can shed more light into the effects of cosmic evolution on properties of individual objects and describe how they change when switching from one model to the other. Or put differently, while in the previous sections we primarily engaged in studying distribution functions, we are now directly testing the influence of our models onto individual objects.

The cross-correlation was performed matching every Λ CDM halo with $M_{200} > 7 \times 10^{13}$ with its counterpart, i.e. 338 haloes were sought in the other models (cf. Table 3). But this mass cut was only applied to the Λ CDM haloes and we were hence able to cross-match every of those Λ CDM haloes. To actually cross-identify objects we used a halo matching technique that correlates those Λ CDM haloes to the halo catalogue of the other models by examining the particle ID lists and maximizing the merit function $C = N_{\text{shared}}^2 / (N_1 N_2)$, where N_{shared} is the number of particles shared by two objects, and N_1 and N_2 are the number of particles in each object, respectively (e.g. Knebe et al. 2013).

For each pair we then compare M_{200} , virialization, spin parameter, mass weighted temperature and gas fraction. The results are all summarized in Fig. 10 and Table 8. Although most of these distribution look quite noisy and scattered about unity, theoretical considerations will give us a key to understand and interpret the (small) deviations observed – to be discussed in the following sub-sections. We only briefly note here that uDE haloes’ parameter do not show, on average, any significant sign of deviation from Λ CDM.

4.1 Virialization

It is known that the degree of virialization of dark matter haloes with kinetic energy K and potential energy U , which is usually defined as

$$\left| \frac{U}{2K} \right| = 1 \quad (22)$$

is affected by the presence of an additional coupling (Abdalla et al. 2010; He et al. 2010). In this case, due to the modification to the standard gravitational potential, the virial relation becomes

$$\left| \frac{U}{2K} \right| = \frac{1 - \xi/2}{1 - 2\xi} \quad (23)$$

where the parameter ξ defined in Abdalla et al. (2010) can be written in terms of our definition of dark matter - dark energy coupling

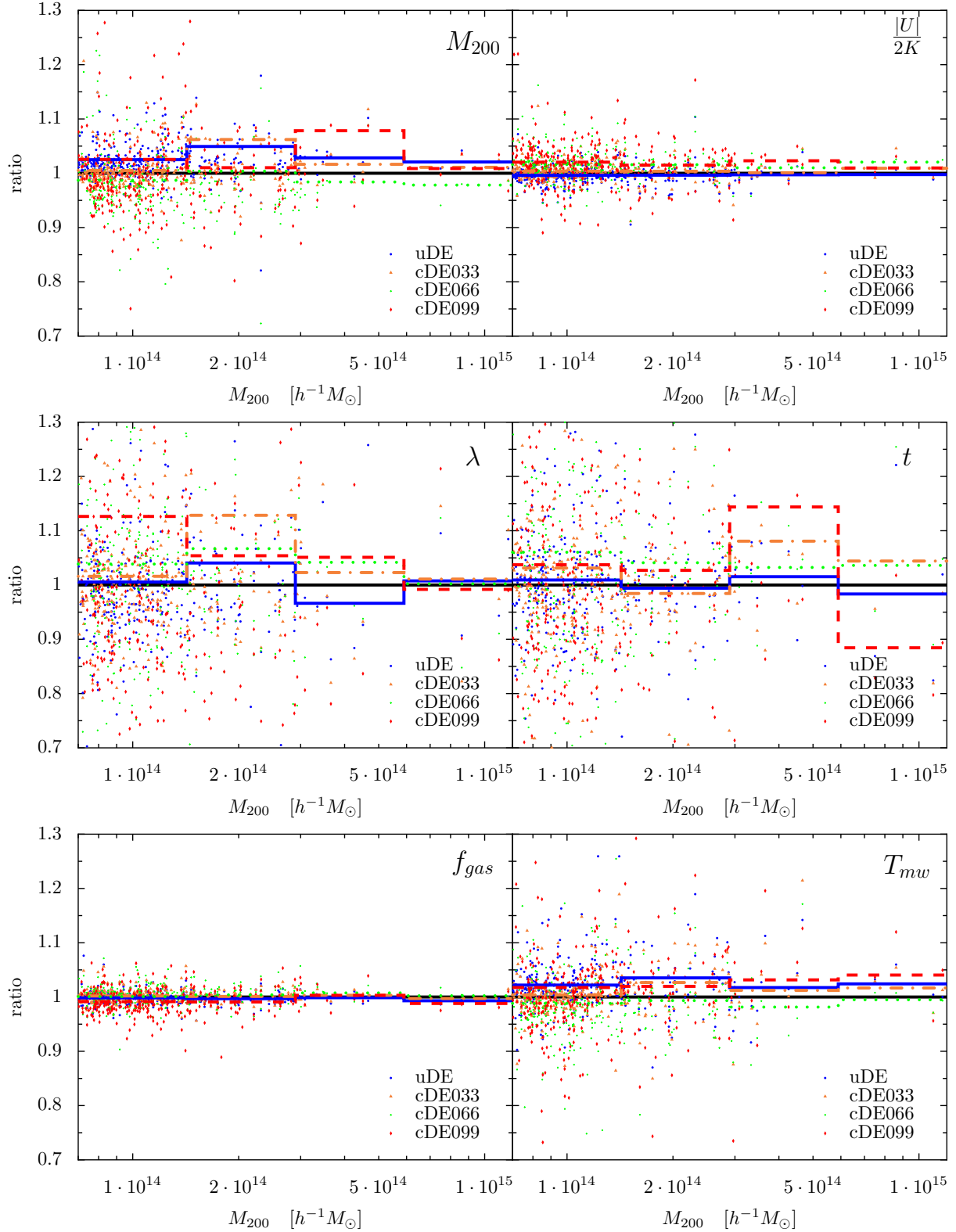


Figure 10. Halo and gas properties in quintessence models. Each dot represents the value of the ratio of the parameter in cDE or uDE to its cross correlated structures in Λ CDM. Upper panels: halo mass (left) and virialization (right). Central panel: halo spin (left) and triaxiality (right). Lower panel: gas fraction (left) and mass-weighted temperature (right).

Table 8. Average of the model to Λ CDM ratio for a series of cross correlated objects with their dispersion. M_{200} is the cross correlated halo mass, $|U|/(2K)$ the ratio of the virialization of each object, T_{mw} the mass weighted temperature, f_{gas} the gas content as a fraction of the total mass, λ the spin parameter and t the triaxiality parameter. Even though the scatter is significant, we can see a correlation of λ , t and virialization to the dark energy coupling, while the other parameters' average are largely independent of the model.

Parameter	uDE	cDE033	cDE066	cDE099
M_{200}	1.03 ± 0.01	1.03 ± 0.03	0.99 ± 0.02	1.04 ± 0.02
$ U /(2K)$	0.997 ± 0.003	1.005 ± 0.005	1.015 ± 0.005	1.05 ± 0.01
T_{mw}	0.998 ± 0.002	1.015 ± 0.004	0.991 ± 0.006	1.03 ± 0.01
f_{gas}	1.029 ± 0.003	1.001 ± 0.001	1.002 ± 0.002	0.991 ± 0.006
λ	1.02 ± 0.04	1.06 ± 0.03	1.05 ± 0.03	1.10 ± 0.04
t	1.01 ± 0.04	1.03 ± 0.02	1.06 ± 0.03	1.05 ± 0.02

as:

$$\xi = \Omega_{dm} \beta_c. \quad (24)$$

We can thus calculate the expected deviation from the standard relation and compare it to the results of Table 8. For cDE099, this value is 1.04, for cDE066 is 1.02 while in cDE033 the value is 1.01. The predictions for these very small deviations from the Λ CDM virial equilibrium are compatible with the average findings of the simulations presented in the upper panel of Fig. 10, although the large scatter does not allow us to draw clear conclusions on the matter. It is however remarkable that, although weak, we can find evidence of this modification.

4.2 Spin parameter

We use the spin parameter as defined by Bullock et al. (2001), i.e.

$$\lambda = \frac{L_{200}}{\sqrt{2} M_{200} V_{200} R_{200}} \quad (25)$$

where the quantities L (the total angular momentum), M (total mass), V (circular velocity) and R (radius) are computed using Eq. (4) with $\Delta = 200$. Our results (shown in the central panel of Fig. 10) indicate that this parameter is positively correlated to the coupling parameter β_c , as already found in the analysis of smaller haloes in cosmologies where dark matter feels an additional force (Hellwing et al. (2011), Paper I). For our models we find that λ in cDE haloes differs on average up to a $\approx 10\%$ from its Λ CDM cross-correlated partner, a result which is in good agreement with the findings of the aforementioned work.

4.3 Triaxiality

We know that the shape of three dimensional haloes can be modelled as an ellipsoidal distribution of particles (Jing & Suto 2002; Allgood et al. 2006), whose three axes are given by the eigenvectors of the inertia tensor defined in Eq. (18). Ordering the corresponding eigenvalues as $a \geq b \geq c$, we define the triaxiality parameter t ³ as

$$t = \frac{a^2 - b^2}{a^2 - c^2}. \quad (26)$$

In Table 8 we observe again a weak dependence of this parameter on β_c in cDE models. cDE haloes here differ to Λ CDM correlated ones by values up to 6%. This effect is not observed at lower

masses (although not shown here), and – like in the previous case – the scatter is quite large so that we definitely need more statistics (i.e. simulations of larger volumes with the same mass resolution) to ensure this is a real feature of massive dark matter haloes in cDE models.

4.4 M_{200} , T_{mw} and f_{gas}

The last halo properties we cross-correlated are mass, gas fraction and mass weighted temperature, shown in the upper and lower panels of Fig. 10. The scatter in the first two is extremely small, with the ratios clustering around unity; T_{mw} on the other hand seem to vary more across models even though still very close to one. Moreover, no sign of dependence on the kind of quintessence or coupling seems to emerge. So, even though we observed that gas and dark matter are distributed differently, it is clear that the integral values of M_{200} and f_{gas} cannot be used as a proxy for these discrepancies. It is interesting to note how the gas fraction, which we found to be strongly correlated to the coupling parameter when projected radially, seems to be now unaffected by the interaction. However, this is not surprising, since a smaller abundance of gas in the central regions of the cluster is expected to have a negligible effect on the overall f_{gas} , due to the little relative weight of the innermost regions. In a typical cluster, the gas mass at $r = 0.1 \times R_{200}$ accounts for only a 3 – 4% of the total, so that changes even as large as 10% only but slightly affect the global balance. In any case, the histories of accretion of these parameters may indeed vary, even bringing about the same results at $z = 0$, as found by Giocoli et al. (2013) in the context of other coupled quintessence models. The behaviour of this quantities at higher redshifts will be analyzed in an upcoming future work.

5 CONCLUSIONS

In this contribution we have studied the properties of clusters and large groups of galaxies using the set of hydrodynamical N -body simulations introduced an earlier work (Paper I). The models under consideration include a fiducial Λ CDM cosmology, an uncoupled Dark Energy (uDE) and three coupled Dark Energy (cDE) models. In each of them we have identified ≈ 330 structures with masses $M_{200} > 7 \times 10^{13} h^{-1} M_{\odot}$ which we further subdivided into smaller subsets to best fit each one of our analysis purposes. The aim was to identify and possibly quantify systematic effects of interacting (cDE) and non-interacting (uDE) quintessence on properties of large and massive structures at $z = 0$, and hence provid-

³ We use t instead of the commonly used T to avoid any confusion with temperatures.

ing a deeper understanding of the phenomenological consequences arising in the non-linear regime of this class of theories.

Our analysis was carried along two conceptually different lines, namely investigating general properties of the set of objects, and then one-to-one comparisons of cross-identified haloes. The first, presented in Section 3, focused upon the determination of the average properties of structures by considering homogeneous samples of objects above a given mass cut. In this way we determined how observables generally behave in different cosmologies. While integrated properties of the clusters, such as the X-ray temperature-mass relation, tend to conceal any dependence on the model, a closer look at the internal structure reveals that cDE models tend to favour less concentrated dark matter haloes and gas fractions which are around 5% below Λ CDM in the innermost regions of the clusters. We interpret this result as a consequence of the reduction of dark matter density in the very same regions, which is also proportional to the coupling. In our case, the suppression is $\approx 10\%$, and is also related to an average increase of the same magnitude of the peak value of the scale radii distribution. This effect was described theoretically by Mainini (2005); Mainini & Bonometto (2006) and later found in N -body simulations for galaxy groups and small clusters by Baldi et al. (2010); Li & Barrow (2011).

The most remarkable findings, however, stem from the study of the radial gas density and pressure profiles. Although we have seen that the extended β model of Mroczkowski et al. (2009) and the observations of pressure profile of Arnaud et al. (2010) seem to be able to account for the numerical results to the same degree, cDE099 and cDE066 still show large differences at the outer cluster edge. In fact, since these properties are related to the ratio $\rho_{gas}(r)/\rho_0$, due to the smaller ρ_0 the ratio becomes larger when approaching R_{200} , and eventually leading to discrepancies $> 20\%$ for pressure profiles, which is so far the largest difference predicted by us and for our models, respectively.

In addition, we have checked that the standard linear relation for temperature profiles in the outskirts of the clusters holds also in the case of uDE and cDE. Even the scatter in the determination of the cluster mass under the hypothesis of hydrostatic equilibrium seems to be largely model independent. However, it remains to be confirmed whether these statements remain when taking into account a larger sample of (even) more massive haloes.

Furthermore, in Section 4 we focused upon individual structures and cross-correlated objects found in the Λ CDM model to their counterparts in the other models. This sort of exercise is strictly theoretical and is aimed at determining which properties of objects forming from comparable initial (Gaussian) conditions and ending up at $z = 0$ in similar environments are most affected and thus likely to keep trace of the cosmological history.

We established that, whereas masses, total gas fractions and mass weighted temperatures do not seem to be affected by cosmology, virialization, spin parameter and triaxiality seem to be dependent on the coupling in the dark sector, albeit only weakly. In particular, we observed that deviations from the standard virial relations are in agreement with the analytical values computed using the formula of Abdalla et al. (2010), while spins seem to follow the pattern found in Paper I at lower mass ranges.

To conclude, we have examined the impact of coupled dark energy in a series of galaxy group and cluster observables at $z = 0$. In some cases, we managed to establish a physical link between the key observational properties and the underlying modified physical laws. However, it is still necessary to study the way background quintessence and scalar field mediated interactions work at higher

redshifts and on larger and more massive structures. This will be the focus of future contributions.

ACKNOWLEDGEMENTS

EC is supported by the *Spanish Ministerio de Economía y Competitividad* (MINECO) under grant no. AYA2012-31101, and Multi-Dark Consolider project under grant CSD2009-00064.

AK is supported by the *Spanish Ministerio de Ciencia e Innovación* (MICINN) in Spain through the Ramón y Cajal programme as well as the grants CSD2009-00064, CAM S2009/ESP-1496 (from the ASTROMADRID network) and the *Ministerio de Economía y Competitividad* (MINECO) through grant AYA2012-31101. He further thanks Jasmine Minks for another age.

GY acknowledges support from MINECO under research grants AYA2012-31101, FPA2012-34694, Consolider Ingenio SyeC CSD2007-0050 and from Comunidad de Madrid under ASTROMADRID project (S2009/ESP-1496).

The authors thankfully acknowledge the computer resources, technical expertise and assistance provided by the Red Española de Supercomputación.

This work was undertaken as part of the Survey Simulation Pipeline (SSimPL: ssimpluniverse.tk) and GFL acknowledges support from ARC/DP 130100117

We further acknowledge partial support from the European Union FP7 ITN INVISIBLES (Marie Curie Actions, PITN-GA-2011-289442).

All the simulations used in this work were performed in the Marenostrum supercomputer at Barcelona Supercomputing Center (BSC).

REFERENCES

- Abdalla E., Abramo L. R., de Souza J. C. C., 2010, *Phys. Rev. D*, 82, 023508
- Allen S. W., Evrard A. E., Mantz A. B., 2011, *Ann.Rev.Astron.Astrophys.*, 49, 409
- Allen S. W., Schmidt R. W., Fabian A. C., 2001, *MNRAS*, 328, L37
- Allgood B., Flores R. A., Primack J. R., Kravtsov A. V., Wechsler R. H., Faltenbacher A., Bullock J. S., 2006, *MNRAS*, 367, 1781
- Ameglio S., Borgani S., Pierpaoli E., Dolag K., Ettori S., Morandi A., 2009, *MNRAS*, 394, 479
- Amendola L., 2000, *Phys. Rev. D*, 62, 043511
- Amendola L., Quercellini C., 2003, *Phys. Rev. D*, 68, 023514
- Arnaud M., 2009, *A&A*, 500, 103
- Arnaud M., Pratt G. W., Piffaretti R., Böhringer H., Croston J. H., Pointecouteau E., 2010, *A&A*, 517, A92
- Bahcall N. A., Lubin L. M., 1994, *ApJ*, 426, 513
- Baldi A., Ettori S., Molendi S., Gastaldello F., 2012, *A&A*, 545, A41
- Baldi M., 2011, *MNRAS*, 411, 1077
- Baldi M., 2012, *MNRAS*, 420, 430
- Baldi M., Lee J., Maccio A. V., 2011, *Astrophys.J.*, 732, 112
- Baldi M., Pettorino V., 2011, *MNRAS*, 412, L1
- Baldi M., Pettorino V., Robbers G., Springel V., 2010, *MNRAS*, 403, 1684
- Baldi M., Salucci P., 2012, *JCAP*, 2, 14
- Baldi M., Viel M., 2010, *MNRAS*, 409, L89
- Bisnovatyi-Kogan G. S., Chernin A. D., 2012, *Ap&SS*, 338, 337

- Bonamente M., et al., 2012, *New Journal of Physics*, 14, 025010
- Bullock J. S., Dekel A., Kolatt T. S., Kravtsov A. V., Klypin A. A., Porciani C., Primack J. R., 2001, *ApJ*, 555, 240
- Caldwell R. R., Dave R., Steinhardt P. J., 1998, *Physical Review Letters*, 80, 1582
- Carlesi E., Knebe A., Lewis G., Yepes G., Wales S., 2013
- Carlesi E., Knebe A., Yepes G., Gottlöber S., Jiménez J. B., Maroto A. L., 2011, *MNRAS*, 418, 2715
- Carlesi E., Knebe A., Yepes G., Gottlöber S., Jiménez J. B., Maroto A. L., 2012, *MNRAS*, 424, 699
- Cavaliere A., Fusco-Femiano R., 1976, *A&A*, 49, 137
- Chiba T., De Felice A., Tsujikawa S., 2013, *Phys. Rev. D*, 87, 083505
- Croston J. H., Pratt G. W., Böhringer H., Arnaud M., Pointecouteau E., Ponman T. J., Sanderson A. J. R., Temple R. F., Bower R. G., Donahue M., 2008, *A&A*, 487, 431
- De Boni C., Dolag K., Ettori S., Moscardini L., Pettorino V., Baccigalupi C., 2011, *MNRAS*, 415, 2758
- De Grandi S., Molendi S., 2002, *ApJ*, 567, 163
- Doran M., 2005, *JCAP*, 10, 11
- Ettori S., De Grandi S., Molendi S., 2002, *A&A*, 391, 841
- Ettori S., Tozzi P., Borgani S., Rosati P., 2004, *A&A*, 417, 13
- Evrard A. E., 1990, *ApJ*, 363, 349
- Gill S. P. D., Knebe A., Gibson B. K., 2004, *MNRAS*, 351, 399
- Giocoli C., Marulli F., Baldi M., Moscardini L., Metcalf R. B., 2013
- He J.-H., Wang B., Abdalla E., Pavon D., 2010, *JCAP*, 12, 22
- Hellwing W. A., Cautun M., Knebe A., Knollmann S., Juszkiewicz R., 2011, *ArXiv e-prints*
- Jing Y. P., Suto Y., 2002, *ApJ*, 574, 538
- Kaiser N., 1986, *MNRAS*, 222, 323
- Knebe A., et al., 2013, *ArXiv e-prints*
- Knollmann S. R., Knebe A., 2009, *ApJS*, 182, 608
- Kravtsov A. V., Borgani S., 2012, *ARA&A*, 50, 353
- Lau E. T., Kravtsov A. V., Nagai D., 2009, *ApJ*, 705, 1129
- Leccardi A., Molendi S., 2008, *A&A*, 486, 359
- Lee J., 2010
- Li B., Barrow J. D., 2011, *MNRAS*, 413, 262
- Macciò A. V., Dutton A. A., van den Bosch F. C., Moore B., Potter D., Stadel J., 2007, *MNRAS*, 378, 55
- Macciò A. V., Quercellini C., Mainini R., Amendola L., Bonometto S. A., 2004, *Phys. Rev. D*, 69, 123516
- Mainini R., 2005, *Phys. Rev. D*, 72, 083514
- Mainini R., Bonometto S., 2006, *Phys. Rev. D*, 74, 043504
- Mangano G., Miele G., Pettorino V., 2003, *Modern Physics Letters A*, 18, 831
- Markevitch M., Forman W. R., Sarazin C. L., Vikhlinin A., 1998, *ApJ*, 503, 77
- Mazzotta P., Rasia E., Moscardini L., Tormen G., 2004, *MNRAS*, 354, 10
- Mroczkowski T., et al., 2009, *ApJ*, 694, 1034
- Muanwong O., Kay S. T., Thomas P. A., 2006, *ApJ*, 649, 640
- Nagai D., Vikhlinin A., Kravtsov A. V., 2007, *ApJ*, 655, 98
- Navarro J. F., Frenk C. S., White S. D. M., 1995, *MNRAS*, 275, 720
- Navarro J. F., Frenk C. S., White S. D. M., 1996, *ApJ*, 462, 563
- Nusser A., Gubser S. S., Peebles P., 2005, *Phys. Rev. D*, 71, 083505
- Pettorino V., Amendola L., Baccigalupi C., Quercellini C., 2012, *Phys. Rev. D*, 86, 103507
- Planck Collaboration Ade P. A. R., Aghanim N., Arnaud M., Ashdown M., Atrio-Barandela F., Aumont J., Baccigalupi C., Balbi A., Banday A. J., et al., 2013, *A&A*, 550, A131
- Prada F., Klypin A. A., Cuesta A. J., Betancort-Rijo J. E., Primack J., 2012, *MNRAS*, 423, 3018
- Rasia E., Tormen G., Moscardini L., 2004, *MNRAS*, 351, 237
- Ratra B., Peebles P. J. E., 1988, *Phys. Rev. D*, 37, 3406
- Samushia L., Ratra B., 2008, *ApJ*, 680, L1
- Sarazin C. L., 1986, *Reviews of Modern Physics*, 58, 1
- Sembolini F., Yepes G., De Petris M., Gottlöber S., Lamagna L., Comis B., 2013, *MNRAS*, 429, 323
- Springel V., 2005, *MNRAS*, 364, 1105
- Springel V., Wang J., Vogelsberger M., Ludlow A., Jenkins A., Helmi A., Navarro J. F., Frenk C. S., White S. D. M., 2008, *MNRAS*, 391, 1685
- Ventimiglia D. A., Voit G. M., Donahue M., Ameglio S., 2008, *ApJ*, 685, 118
- Vikhlinin A., Forman W., Jones C., 1999, *ApJ*, 525, 47
- Vikhlinin A., Kravtsov A., Forman W., Jones C., Markevitch M., Murray S. S., Van Speybroeck L., 2006, *ApJ*, 640, 691
- Vikhlinin A., Markevitch M., Murray S. S., Jones C., Forman W., Van Speybroeck L., 2005, *ApJ*, 628, 655
- Wang P.-Y., Chen C.-W., Chen P., 2012, *JCAP*, 2, 16
- Wetterich C., 1995, *A&A*, 301, 321
- Zlatev I., Wang L., Steinhardt P. J., 1999, *Physical Review Letters*, 82, 896

This paper has been typeset from a $\text{\TeX}/\text{\LaTeX}$ file prepared by the author.